Hindawi
Geofluids
Volume 2020, Article ID 6531254, 13 pages
https://doi.org/10.1155/2020/6531254

Research Article

Pressure-Predicting Model for Ultralow-Permeability Reservoirs considering the Water Absorption Characteristics of Mudstone Formations

Kai Liu,[1,2] Daiyin Yin ,[1,2] and Yong Wang[3]

[1]*Department of Petroleum Engineering, Northeast Petroleum University, Daqing, Heilongjiang Province 163318, China*
[2]*Key Laboratory of the Ministry of Education for Improving Oil and Gas Recovery, Northeast Petroleum University, Daqing, Heilongjiang Province 163318, China*
[3]*Shengli Oilfield Exploration and Development Research Institute, Dongying, Shandong Province 257000, China*

Correspondence should be addressed to Daiyin Yin; yindaiyin@nepu.edu.cn

Received 31 August 2019; Revised 23 April 2020; Accepted 14 May 2020; Published 14 June 2020

Academic Editor: Ye Zhang

The injection-production ratio of ultralow-permeability reservoirs is generally higher in the early stage of development because of the water absorption characteristics of transition layers and mudstone formations. In this paper, the water absorption characteristics of mudstone are experimentally studied, and the empirical function of the water absorption process is established. A new mathematical model of the whole lithology is established by applying the research results of mudstone water absorption characteristics. Combining the material balance method and finite difference method, the space terms in the basic differential equation are replaced by the material balance equation, and the finite difference in the time term is obtained. Then, the analytical solutions of the average pressures of the reservoir oil well area, reservoir water well area, transition layers, and mudstone formations are solved. Based on the static parameters of the reservoir in the Chaoyang Gou Oilfield of the ultralow-permeability reservoir in China, the new pressure prediction model is verified by the ideal model of numerical simulation and production data of the oil field. The experimental results show that the saturation water absorption rate of mudstone is 1.54-2.55%, and the water absorption process of mudstone cannot be described by the seepage equation of sandstone. The verification results of the numerical simulation show that the pressure of the transition layers and mudstone at the end of the water well gradually increases, while the pressure at the end of the oil well basically remains unchanged, which is consistent with the assumptions of the model. The verification results of the oilfield production data show that the water well static pressure and oil well static pressure calculated by the new model are highly consistent with the actual values, which well explains the phenomenon of the low reservoir pressure level under the condition of a high injection production ratio in an ultralow-permeability reservoir.

1. Introduction

Due to the water absorption characteristics of transition layers and overlying mudstone formations, the injection-production ratio of ultralow-permeability reservoirs is usually greater than 1 at the initial stage of development, and the change law of reservoir pressure is quite different from that of conventional reservoirs [1–4]. The material balance method and numerical simulation method are commonly used research methods to solve these problems. Liu et al. and Fan et al. studied the variation of reservoir pressure around water wells in ultralow-permeability reservoirs at different injection-production ratio conditions using numerical simulation [5, 6]. Johnson and Rodgerson theoretically deduced the formula to calculate the pressure field around the crack in infinite elasticity [7]. Yin et al. used the finite element method to simulate the borehole wallrock stress field and pressure field evolution in the relief process [8]. Zou et al. deduced the injection-production ratio model of low-permeability reservoirs for balanced and unbalanced systems

based on the extreme value principle [9]. Wu qualitatively analysed that the abnormally high injection-production ratio in low-permeability reservoirs was caused by ineffective water injection and presented the ineffective water absorption volume that accounted for 28.3% of the total water volume according to experience [10]. However, these scholars did not quantitatively introduce the water absorption characteristics of mudstone into the calculation model.

Scholars at home and abroad have conducted many experiments on water absorption characteristics of mudstone [2, 11–17]. Erguler and Ulusay selected different types of mudstone cores from different parts of Turkey to conduct mudstone water absorption experiments. The water absorption process of mudstone was divided into the isokinetic water absorption stage, accelerated water absorption stage, and isokinetic water absorption stage, but the function of the water absorption process was not provided [18]. Jiang et al. verified the water absorption characteristics of mudstone and analysed the corresponding influencing factors using computerized tomographic scanning [19]. Li et al. selected mudstone samples from Tibet for water absorption experiments and scanning electron microscopy (SEM) tests. They presented an inflection point on the water absorption curve [20]. Guo et al. studied the water absorption capacity of mudstone using the self-developed intelligent testing system for water absorption of deep soft rock [21]. He et al. also presented that the mudstone with high water invasion pressure (the situation of high injection-production ratio at the early stage of development of ultralow-permeability reservoirs) had stronger water absorption capacity than non-pressure water absorption [22].

In this paper, the water absorption characteristics of mudstone are analysed by taking mudstone water absorption experiments, and the relation between the mudstone water absorption rate and water invasion pressure is quantified by establishing an empirical function of the water absorption process. Furthermore, a mathematical model of whole lithologic pressure diffusion considering the transition reservoir and mudstone formation is established. The model can reflect the effect of water absorption characteristics of the transition layers and overlying mudstone formations on pressure in ultralow-permeability reservoirs. Moreover, it can more accurately predict the average formation pressure to determine a reasonable injection-production ratio.

2. Water Absorption Characteristics of Mudstone

The water absorption characteristics of mudstone at different water invasion pressures are studied by water absorption experiments of mudstone. The empirical function for the water absorption process of mudstone is established based on the experimental results.

2.1. Water Absorption Experiment of Pure Mudstone. The water absorption characteristics of mudstone at different water invasion pressures are studied by taking the mudstone cores of inspection wells in Chaoyang Gou Oilfield of an ultralow-permeability reservoir as the experimental object.

2.1.1. Experimental Materials and Processes. The core samples in the experiment are taken from the inspection wells in Block S of ultralow-permeability reservoirs in China. The X-ray diffraction analysis results of the inspection well core samples are statistically analysed; the basic parameters and compositions of the core samples are shown in Table 1.

The flow chart of the mudstone water absorption experiment is shown in Figure 1. The specific flow chart is as follows.

S01: core samples and determination of basic parameters. The drilled core samples were placed in a constant temperature box at 60°C for two weeks until the difference between weighings was less than 1%. Then, the permeability was measured with nitrogen.

S02: the core sample is put into the core holder, and the core holder is placed on the electronic scale, which is convenient for measuring the water absorption flux at different times. After connecting the pipeline, formation water is recharged from the outlet to the core, then the back-pressure valve is closed, and the pressure gauge is connected at the outlet.

S03: the flow pump is set in constant pressure displacement mode. The same confining pressure is loaded by the confining pressure controller, and the displacement pressure is set to the pump according to the experimental scheme. The experiment is started, and the accumulated water absorption flux is recorded at different times until the accumulated flow flux is basically unchanged, and the experiment is finished.

S04: in the experimental results, the cumulative water absorption flux is calculated and recorded according to the weight of the electronic scales at different times. At the initial stage of mudstone water absorption, data are recorded every 2 hours; after the mudstone water absorption is stable, data are recorded every 6 hours. After the experiment, the maximum water absorption flux of mudstone with constant water invasion pressure is recorded, and the saturation water absorption is calculated.

2.1.2. Experimental Result. The saturation water absorption flux (maximum water absorption flux with constant water invasion pressure) and saturation water absorption rate (ratio of saturation water absorption flux to core sample volume with constant water invasion pressure) are obtained by mudstone water absorption experiments. To provide an experimental data basis for establishing an empirical function of the mudstone water absorption process, 7 types of water invasion pressures are set, and 3 cores are made for each type of water invasion pressure. The experimental results are shown in Table 2. Taking one core as an example for each type of water invasion pressure, the curves of water absorption characteristics are shown in Figure 2.

According to the experimental results, the water absorption characteristics of mudstone are as follows. (i) When the water invasion pressure is constant, the water absorption rate increases with the increase in water absorption time, but the increase rate gradually decreases and finally remains basically unchanged. (ii) A higher water invasion pressure

Table 1: Basic parameters and compositions of core samples from the inspection wells.

Core number	Length (cm)	Diameter (cm)	Permeability ($10^{-3}\mu m^2$)	Porosity (%)	Mineral type and content (%)			Clay content (%)
					Quartz	Potash feldspar	Soda feldspar	
M-1	8.2	2.5	0.012	4.2	26.6	3.2	17.6	52.6
M-2	7.8	2.5	0.016	3.3	25.7	2.8	22.9	48.6
M-3	7.4	2.5	0.015	3.2	27.2	1.7	19.4	51.7
M-4	7.6	2.5	0.009	4.7	29.1	3.2	16.6	51.1
M-5	7.7	2.5	0.007	4.2	28.6	3.9	17.7	49.8
M-6	7.8	2.5	0.011	3.8	22.8	2.2	27.4	47.6
M-7	7.9	2.5	0.006	3.9	27.2	2.4	21.6	48.8
M-8	8	2.5	0.011	5.1	26.1	1.8	22.9	49.2
M-9	7.6	2.5	0.01	4.5	23.9	3.3	22.6	50.2
M-10	7.8	2.5	0.008	4.6	24.5	2.6	22.1	50.8
M-11	8.2	2.5	0.009	3.1	25.4	4.2	19.1	51.3
M-12	8.1	2.5	0.007	3.5	27.5	3.3	13.8	55.4
M-13	7.7	2.5	0.012	3.9	27.8	2.7	18.3	51.2
M-14	7.8	2.5	0.013	3.7	25.2	2.9	21.6	50.3
M-15	7.9	2.5	0.008	4.1	24.4	3.4	24.1	48.1
M-16	8.1	2.5	0.016	4.4	25.7	3.7	21.9	48.7
M-17	8	2.5	0.008	3.2	24.9	4.1	21.4	49.6
M-18	7.9	2.5	0.011	4	25.7	2.6	22.5	49.2
M-19	7.8	2.5	0.006	3.8	23.6	2.3	22.9	51.2
M-20	7.9	2.5	0.014	3.6	29.2	2.1	16.4	52.3
M-21	8.2	2.5	0.006	4.5	27.1	3.1	19.1	50.7

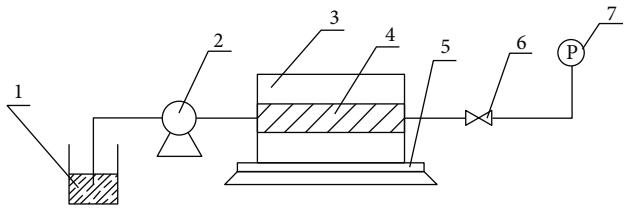

Figure 1: Flow chart of the water absorption experiment: 1: liquid reservoir; 2: plunger pump; 3: core holder; 4: mudstone core; 5: electronic scale; 6: back-pressure valve; 7: pressure gauge.

corresponds to higher saturation water absorption and more time required for water absorption to reach saturation. (iii) During the experiment, the pressure at the end of the core sample remains at the initial pressure of 0.1 MPa, which indicates that the water absorption velocity through the cross-section of the mudstone core is very low, and no water flows through the end of the core until the water absorption reaches saturation. Therefore, the water absorption process of mudstone is different from that of sandstone seepage, and the seepage equation cannot be used to describe the water absorption characteristics of mudstone.

2.2. Empirical Function of Water Absorption Process. Based on the experimental results of mudstone water absorption and the references [23, 24], the water absorption process function is determined. According to Figure 2, the water absorption characteristic curve of mudstone shows a negative exponential complex function relation.

$$R_{ws} = R_{wsm}\left(1 - e^{-\delta t}\right), \quad (1)$$

where R_{ws} is the water absorption rate, which varies with the water invasion pressure and time, %; R_{wsm} is the saturation water absorption rate, %; δ is the water absorption attenuation coefficient, d^{-1}; and t is the water absorption time, d.

2.2.1. Relation between Saturation Water Absorption Rate and Water Invasion Pressure. The logarithmic relation between saturation water absorption rate and water invasion pressure is determined by fitting the statistical data of the saturation water absorption rate at different water invasion pressures. The results are shown in Figure 3.

$$R_{wsm} = 0.0061 \ln\left(\frac{P}{P_i}\right), \quad (2)$$

where P is the water invasion pressure, MPa; P_i is the initial pressure, MPa.

2.2.2. Relation between Water Absorption Attenuation Coefficient and Water Invasion Pressure. The power function relation between the water absorption attenuation coefficient and water invasion pressure is determined by fitting the statistical data of the water absorption attenuation coefficient

Table 2: Experimental results of the mudstone water absorption.

Core number	Volume (cm^3)	Water invasion pressure (MPa)	Saturation water absorption time (d)	Saturation water absorption flux (cm^3)	Saturated water absorption rate (%)
M-1	40.23	4	8.5	0.76	1.88
M-2	38.27	4	8.5	0.69	1.81
M-3	36.31	4	8.5	0.64	1.76
M-4	37.29	6	14.0	0.71	1.91
M-5	37.78	6	13.5	0.75	1.98
M-6	38.27	6	13.5	0.78	2.04
M-7	38.76	8	15.0	0.84	2.16
M-8	39.25	8	15.5	0.87	2.22
M-9	37.29	8	15.5	0.80	2.14
M-10	38.27	10	18.0	0.88	2.31
M-11	40.23	10	18.0	0.94	2.34
M-12	39.74	10	18.5	0.95	2.38
M-13	37.78	12	20.5	0.94	2.48
M-14	38.27	12	21.5	0.92	2.41
M-15	38.76	12	21.5	0.97	2.49
M-16	39.74	14	23.5	1.00	2.51
M-17	39.25	14	24.5	1.01	2.58
M-18	38.76	14	23.5	0.99	2.55
M-19	38.27	16	24.5	1.00	2.62
M-20	38.76	16	25.0	1.01	2.61
M-21	40.23	16	24.0	1.06	2.64

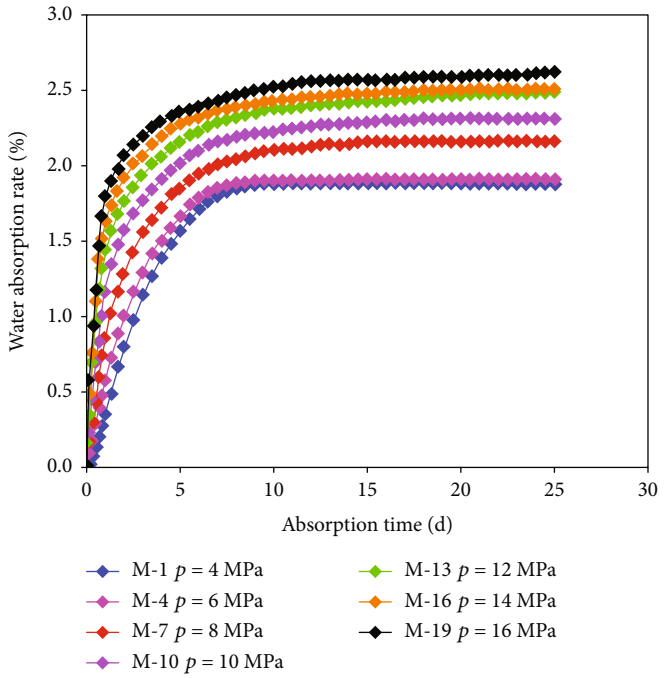

Figure 2: Water absorption characteristic curve of mudstone in an inspection well.

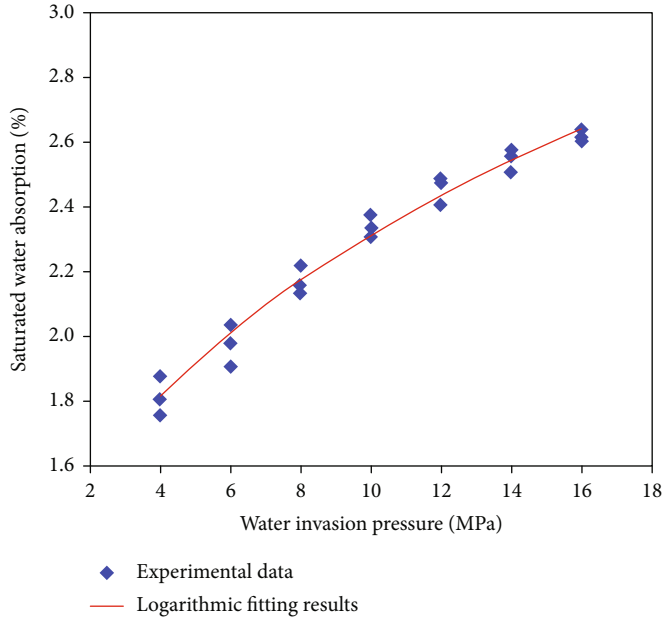

Figure 3: Relation between saturation water absorption and water invasion pressure.

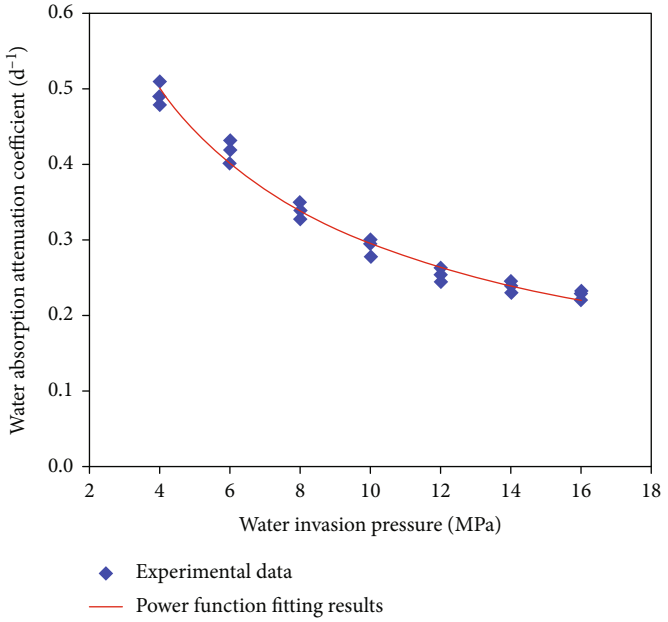

Figure 4: Relation between water absorption attenuation coefficient and water invasion pressure.

at different water invasion pressures. The results are shown in Figure 4.

$$\delta = 1.1327(P - P_i)^{-0.5896}. \tag{3}$$

Therefore, the empirical formulas of cumulative water influx (Q) and instantaneous water influx (q) are obtained.

$$Q = 0.0061 \ln\left(\frac{P}{P_i}\right)\left(1 - e^{-1.1327(P-P_i)^{-0.5896}t}\right) \cdot S \cdot d, \tag{4}$$

$$q = \frac{dQ}{dt} = 0.0061 \ln\left(\frac{P}{P_i}\right) \cdot \left[1.1327(P - P_i)^{-0.5896}\right] \cdot e^{-1.1327(P-P_i)^{-0.5896}t} \cdot S \cdot d. \tag{5}$$

Then, the velocity of water invasion per unit cross-sectional area is

$$q = 0.0061 \ln\left(\frac{P}{P_i}\right) \cdot \left[1.1327(P - P_i)^{-0.5896}\right] \cdot e^{-1.1327(P-P_i)^{-0.5896}t} \cdot d, \tag{6}$$

where S is the cross-sectional area of mudstone core, m^2; d is the distance perpendicular to the cross-section, m. According to Equation (6), the velocity of water invasion per unit cross-sectional area of mudstone is related to the pressure of water invasion and the thickness of the mudstone layer, which provides a basis for solving the whole lithologic pressure diffusion mathematical model.

3. Mathematical Model of Pressure Diffusion for Whole Lithology

Taking an injection-production unit as the research object, i.e., a group of wells consisting of a central injection well and surrounding oil-water wells, we provide an example of the inverse nine-point well pattern.

Vertically, considering the water absorption characteristics of transition layers and mudstone formations, the geological model is divided into three parts: sandstone reservoir, transition layers, and mudstone formations. The cylindrical coordinate system is established with the central well as its pole, as shown in Figure 5.

The mathematical model established in this paper makes the following assumptions: (1) For reservoirs, there are a horizontal radial flow to oil wells and a vertical flow to the transition layers in the control area of water wells, while there is only a horizontal radial flow to oil wells in the control area of oil wells. (2) For transition layers and mudstone formations, there is only a vertical flow of injected water. (3) Both transition lithology and sandy mudstone have permeability, and the flow flux is calculated according to Darcy's formula, while the water absorption flux is calculated according to the established empirical formula. (4) In the early stage of ultralow-permeability reservoir development, a clay stabilizer is injected at the same time of the water injection to prevent the clay from swelling and hydration migration from blocking the throat, so it is assumed that the permeability does not change during water injection.

Taking the reservoir as the research object, the continuity equation is established as follows considering the point source of the water well, point sink of the oil well, and transfer between reservoir and transition layers.

$$-\frac{\partial v_r}{\partial r}-\frac{1}{r}v_r-\frac{\partial v_{z1}}{\partial z}+\sum_{i=1}^{N_w}q_{wi}\delta(r-r_i)-\sum_{j=1}^{N_o}q_{lj}\delta(r-r_j)-q_{k1}\delta(z-z_1)=C_{e1}\varphi_1\frac{\partial p_1}{\partial t}. \tag{7}$$

Taking the transition lithology in transition layers as the research object, the fluid continuity equation is

$$-\frac{\partial v_{z2}}{\partial z}+q_{k1}\delta(z-z_1)-q_{k2}\delta(z-z_2)=C_{e2}\frac{\partial p_2}{\partial t}. \tag{8}$$

Taking sandy mudstone in transition layers as the research object, the fluid continuity equation is as follows:

$$\frac{\partial v_{z3}}{\partial z}+q_{k2}\delta(z-z_2)-q_{k3}\delta(z-z_3)-q_{k4}=C_{e3}\varphi_3\frac{\partial p_3}{\partial t}. \tag{9}$$

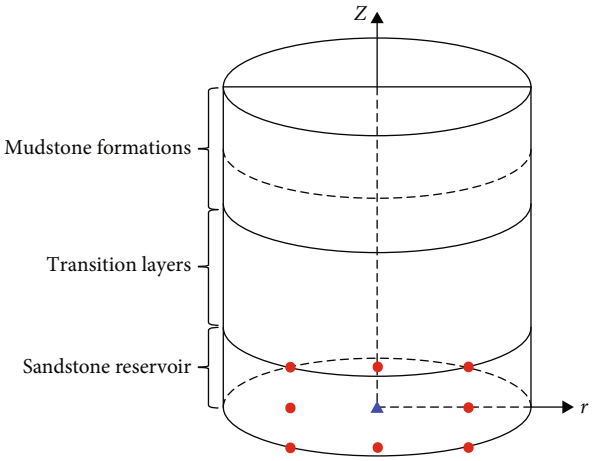

Figure 5: Geological model of the whole lithology in the cylindrical coordinate system.

The seepage equation considering the start-up pressure gradient is as follows:

$$v_r=-\frac{k}{\mu}\left(\frac{\partial p}{\partial r}-D_p\right), \tag{10a}$$

$$v_z=-\frac{k}{\mu}\left(\frac{\partial p}{\partial r}-D_p\right). \tag{10b}$$

The pressure diffusion mathematical model considering the water absorption characteristics of the transition layers and overlying mudstone is obtained by substituting Equations (10a) and (10b) into Equations (7), (8), and (9).

For reservoirs,

$$\frac{\partial}{\partial r}\left[\frac{k_1}{\mu}\left(\frac{\partial p_1}{\partial r}-D_{p1}\right)\right]+\frac{1}{r}\frac{k_1}{\mu}\left(\frac{\partial p_1}{\partial r}-D_{p1}\right)+\frac{\partial}{\partial z}\left[\frac{k_1}{\mu}\left(\frac{\partial p_1}{\partial r}-D_{p1}\right)\right]+q_{wi}\delta(r-r_i)-q_L\delta(r-r_j)-q_{z1}\delta(z-z_1)=C_{e1}\phi_1\frac{\partial p_1}{\partial t}. \tag{11a}$$

For transition lithology,

$$-\frac{\partial}{\partial z}\left[\frac{k_2}{\mu}\left(\frac{\partial p_2}{\partial z}-D_{p2}\right)\right]+q_{z1}\delta(z-z_1)-q_{z2}\delta(z-z_2)=C_{e2}\frac{\partial p_2}{\partial t}. \tag{11b}$$

For sandy mudstone,

$$-\frac{\partial}{\partial z}\left[\frac{k_3}{\mu}\left(\frac{\partial p_3}{\partial z}-D_{p3}\right)\right]+q_{z2}\delta(z-z_2)-q_{z3}\delta(z-z_3)-q_{z4}=C_{e3}\frac{\partial p_3}{\partial t}. \tag{11c}$$

The initial condition is

$$p_{1(r,z)}=p_{Li},\quad p_{2(r,z)}=p_{2i},\quad p_{3(r,z)}=p_{3i}. \tag{12}$$

The boundary condition is

$$\left.\frac{\partial p_3}{\partial z}\right|_{z=z_3} = 0. \tag{13}$$

4. Solution of the Mathematical Model

The pressure diffusion mathematical model is a set of partial differential Equation (5), which cannot directly derive analytical solutions. To solve this type of equations, there are two main methods: numerical difference method and simplifying the treatment to obtain analytical formulas. The former must compile a complex simulation software, while the current commercial numerical simulation software cannot equivalently handle mudstone water absorption characteristics. In this paper, the second method is used to simplify the geological model into two zones: the seepage zone in the control area of the water well and the seepage zone in the control area oil well. The schematic diagram is shown in Figure 6.

After oil wells are put into production, the reservoir pressure in the area controlled by oil wells decreases and the increases, which will cause the underground fluid transfer from the water well to the reservoir controlled by oil wells and transition lithologic. Combined with the material balance method, the partial differential Equations (11a), (11b) and (11c) can be rewritten into ordinary differential equations.

For the controlled area of water well in the reservoir,

$$\frac{d\bar{p}_{1w}}{dt} = \frac{1}{V_{w1}\varphi_1 C_{e1}}\left[q_w - \lambda_1\left(\bar{p}_{1w} - \bar{p}_{1o} - D_{p1}\cdot L\right) - 2q_{z1}\right]. \tag{14a}$$

For the controlled area of oil well in the reservoir,

$$\frac{d\bar{p}_{1o}}{dt} = \frac{1}{V_{o1}\varphi_1 C_{e1}}\left[\lambda_1\left(\bar{p}_{1w} - \bar{p}_{1o} - D_{p1}\cdot L\right) - q_L\right]. \tag{14b}$$

For transition lithology in the transition layers,

$$\frac{d\bar{p}_{2w}}{dt} = \frac{1}{V_{w2}C_{e2}}\left[q_{z1} - q_{z2}\right]. \tag{14c}$$

For sandy mudstones in the transition layers

$$\frac{d\bar{p}_{3w}}{dt} = \frac{1}{V_{w3}C_{e3}}\left[q_{z2} - q_{z3} - q_{z4}\right]. \tag{14d}$$

The volume flow velocity (q_{z1}) from the reservoir to the transition lithology in the water well controlled area is

$$q_{z1} = S_1\cdot\frac{\overline{k_1}}{\mu_w}\left[\frac{\bar{P}_{1w} - \bar{P}_{2w}}{d_1} - \bar{D}_{p1}\right]. \tag{15a}$$

The volume flow velocity (q_{z2}) from the reservoir to the transition lithology in the water well controlled area is

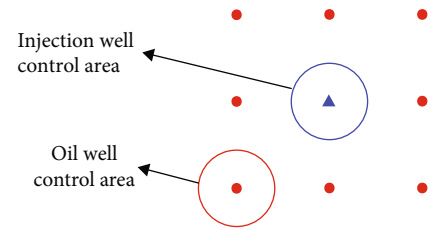

Figure 6: Schematic diagram of the seepage area of oil and water wells.

$$q_{z2} = S_2\cdot\frac{\overline{k_2}}{\mu_w}\left[\frac{\bar{P}_{2w} - \bar{P}_{3w}}{d_2} - \bar{D}_{p2}\right]. \tag{15b}$$

According to the empirical Equation (6) of mudstone water absorption, the volume flow velocity from sandy mudstone to mudstone in the water well controlled area is

$$q_{z3} = 0.0061\ln\left(\frac{P}{P_i}\right)\cdot\left[1.1327(P - P_i)^{-0.5896}\right] \cdot e^{-1.1327(P-P_i)^{-0.5896}t}\cdot d, \tag{15c}$$

where the conductivity (λ) can be expressed as

$$\lambda_1 = \left(\frac{k_{ro}}{\mu_o} + \frac{k_{rw}}{\mu_w}\right)\frac{A}{L}. \tag{16}$$

The intermediate transfer cross-section area in an oil well controlled area can be expressed as

$$S_1 = S_2 = S_3 = \pi r_e^2. \tag{17}$$

The average permeability can be obtained by weighing the reservoir thickness.

$$\bar{k}_1 = \frac{h_1k_1 + h_2k_2}{\mu_w(h_1 + h_2)}, \tag{18a}$$

$$\bar{k}_2 = \frac{h_2k_2 + h_3k_3}{\mu_w(h_2 + h_3)}. \tag{18b}$$

The average threshold pressure gradient can be obtained by weighing the reservoir thickness.

$$\bar{D}_{p1} = \frac{h_1D_{p1} + h_2D_{p2}}{h_1 + h_2}, \tag{19a}$$

$$\bar{D}_{p2} = \frac{h_2D_{p2} + h_3D_{p3}}{h_2 + h_3}. \tag{19b}$$

The average distance of longitudinal intermediate transfer can be expressed as

$$d_1 = 0.5(h_1 + h_2), \tag{20a}$$

$$d_2 = 0.5(h_2 + h_3), \tag{20b}$$

$$d_3 = 0.5h_3. \tag{20c}$$

Let the parameter group be

$$\alpha_1 = \frac{1}{V_{w1}\varphi_1 C_{e1}},\ \alpha_2 = \frac{1}{V_{w2}C_{e2}},\ \alpha_3 = \frac{1}{V_{w3}C_{e3}}, \tag{21}$$

$$B = \frac{q_w}{q_L}, \tag{22}$$

$$\lambda_{z1} = S_1 \cdot \frac{\bar{k}_1}{\mu_w},\ \lambda_{z2} = S_2 \cdot \frac{\bar{k}_2}{\mu_w},\ \lambda_{z3} = S_3 \cdot 0.0061\alpha e^{-\alpha t} \cdot d_3. \tag{23}$$

After substituting Equations (15a), (15b), (15c), (16), (17), (18a), (18b), (19a), (19b), (20a), (20b) and (20c) and the parameter groups (Equations (21), (22) and (23)) into the simplified pressure diffusion model (Equations (14a), (14b), (14c) and (14d)), the equations can be simplified.

$$\frac{d\bar{p}_{1w}}{dt} = \alpha_1\left[B \cdot q_L - \lambda_1\left(\bar{p}_{1w} - \bar{p}_{1o} - D_{p1} \cdot L\right) - 2\lambda_{z1}\left(\bar{P}_{1w} - \bar{P}_{2w} - \bar{D}_{p1} \cdot d_1\right)\right], \tag{24a}$$

$$\frac{d\bar{p}_{1o}}{dt} = \alpha_1\left[\lambda_1\left(\bar{p}_{1w} - \bar{p}_{1o} - D_{p1} \cdot L\right) - q_L\right], \tag{24b}$$

$$\frac{d\bar{p}_{2w}}{dt} = \alpha_2\left[\lambda_{z1}\left(\bar{P}_{1w} - \bar{P}_{2w} - \bar{D}_{p1} \cdot d_1\right) - \lambda_{z2}\left(\bar{P}_{2w} - \bar{P}_{3w} - \bar{D}_{p2} \cdot d_2\right)\right], \tag{24c}$$

$$\frac{d\bar{p}_{3w}}{dt} = \alpha_3\left[\lambda_{z2}\left(\bar{P}_{2w} - \bar{P}_{3w} - \bar{D}_{p2} \cdot d_2\right) - \lambda_{z3}\ln\left(\frac{\bar{P}_{3w}}{P_i}\right) - q_{z4}\right]. \tag{24d}$$

The differential term at the left end of Equations (24a), (24b), (24c) and (24d) is replaced by the difference term, and the pressure at the right end of the equation is replaced by the variable of time $n + 1$.

$$\frac{d\bar{p}_{1w}}{dt} = \frac{\bar{p}_{1w}^{n+1} - \bar{p}_{1w}^{n}}{\Delta t},\ \frac{d\bar{p}_{1o}}{dt} = \frac{\bar{p}_{1o}^{n+1} - \bar{p}_{1o}^{n}}{\Delta t},\ \frac{d\bar{p}_{2w}}{dt} = \frac{\bar{p}_{2w}^{n+1} - \bar{p}_{2w}^{n}}{\Delta t},\ \frac{d\bar{p}_{3w}}{dt} = \frac{\bar{p}_{3w}^{n+1} - \bar{p}_{3w}^{n}}{\Delta t}, \tag{25a}$$

$$\bar{p}_{1w} = \bar{p}_{1w}^{n+1},\ \bar{p}_{1o} = \bar{p}_{1o}^{n+1},\ \bar{p}_{2w} = \bar{p}_{2w}^{n+1},\ \bar{p}_{3w} = \bar{p}_{3w}^{n+1}. \tag{25b}$$

The equation group about $\bar{p}_{1o}^{n+1}$, $\bar{p}_{1w}^{n+1}$, $\bar{p}_{2w}^{n+1}$, and $\bar{p}_{3w}^{n+1}$ is obtained by substituting Equationa (25a) and (25b) into Equations (24a), (24b), (24c) and (24d), which has exactly four unknown variables. The average pressure in different parts can be obtained by solving the equation group.

$$\left(\frac{1}{\alpha_1\Delta t} + \lambda_1 + 2\lambda_{z1}\right)\bar{p}_{1w}^{n+1} - \lambda_1\bar{p}_{1o}^{n+1} - 2\lambda_{z1}\bar{p}_{2w}^{n+1} = \frac{1}{\alpha_1\Delta t}\bar{p}_{1w}^{n} + B \cdot q_L + \lambda_1 \cdot D_{p1} \cdot L + 2\lambda_{z1} \cdot \bar{D}_{p1} \cdot d_1, \tag{26a}$$

$$-\lambda_1\bar{p}_{1w}^{n+1} + \left(\frac{1}{\alpha_1 \cdot \Delta t} + \lambda_1\right)\bar{p}_{1o}^{n+1} = \frac{1}{\alpha_1 \cdot \Delta t}\bar{p}_{1o}^{n} - q_L - \lambda_1 \cdot D_{p1} \cdot L, \tag{26b}$$

$$\lambda_{z1}\bar{p}_{1w}^{n+1} - \left(\frac{1}{\alpha_2\Delta t} + \lambda_{z1} + \lambda_{z2}\right)\bar{p}_{2w}^{n+1} + \lambda_{z2}\bar{p}_{3w}^{n+1} = -\frac{1}{\alpha_2\Delta t}\bar{p}_{2w}^{n} + \lambda_{z1} \cdot \bar{D}_{p1} \cdot d_1 - \lambda_{z2} \cdot \bar{D}_{p2} \cdot d_2, \tag{26c}$$

$$-\lambda_{z2}\bar{p}_{2w}^{n+1} + \left(\frac{1}{\alpha_3 \cdot \Delta t} + \lambda_{z2}\right)\bar{p}_{3w}^{n+1} = \frac{1}{\alpha_3 \cdot \Delta t}\bar{p}_{3w}^{n} - \lambda_{z3}\ln\left(\frac{\bar{p}_{3w}^{n}}{p_i}\right) - \lambda_{z2} \cdot \bar{D}_{p2} \cdot d_2 - q_{z4}. \tag{26d}$$

Let the constant terms be

$$a_1 = \frac{1}{\alpha_1\Delta t} + \lambda_1 + 2\lambda_{z1},\ b_1 = \frac{1}{\alpha_1\Delta t}\bar{p}_{1w}^{n} + B \cdot q_L + \lambda_1 \cdot D_{p1} \cdot L + 2\lambda_{z1} \cdot \bar{D}_{p1} \cdot d_1, \tag{27a}$$

$$a_2 = \frac{1}{\alpha_1 \cdot \Delta t} + \lambda_1,\ b_2 = \frac{1}{\alpha_1 \cdot \Delta t}\bar{p}_{1o}^{n} - q_L - \lambda_1 \cdot D_{p1} \cdot L, \tag{27b}$$

$$a_3 = \frac{1}{\alpha_2\Delta t} + \lambda_{z1} + \lambda_{z2},\ b_3 = -\frac{1}{\alpha_2\Delta t}\bar{p}_{2w}^{n} + \lambda_{z1} \cdot \bar{D}_{p1} \cdot d_1 - \lambda_{z2} \cdot \bar{D}_{p2} \cdot d_2, \tag{27c}$$

$$a_4 = \frac{1}{\alpha_3 \cdot \Delta t} + \lambda_{z2},\ b_4 = \frac{1}{\alpha_3 \cdot \Delta t}\bar{p}_{3w}^{n} - \lambda_{z3}\ln\left(\frac{\bar{p}_{3w}^{n}}{p_i}\right) - \lambda_{z2} \cdot \bar{D}_{p2} \cdot d_2 - q_{z4}. \tag{27d}$$

The above equation can be rewritten as follows:

$$a_1\bar{p}_{1w}^{n+1} - \lambda_1\bar{p}_{1o}^{n+1} - 2\lambda_2\bar{p}_{2w}^{n+1} = b_1, \tag{28a}$$

$$-\lambda_1\bar{p}_{1w}^{n+1} + a_2\bar{p}_{1o}^{n+1} = b_2, \tag{28b}$$

$$\lambda_{z1}\bar{p}_{1w}^{n+1} - a_3\bar{p}_{2w}^{n+1} + \lambda_{z2}\bar{p}_{3w}^{n+1} = b_3, \tag{28c}$$

$$-\lambda_{z2}\bar{p}_{2w}^{n+1} + a_4\bar{p}_{3w}^{n+1} = b_4. \tag{28d}$$

The average reservoir pressure in the water well controlled area is calculated as follows:

$$\bar{p}_{1w}^{n+1} = \frac{2a_2\lambda_2(b_3a_4 - b_4\lambda_{z2}) - (b_1a_2 + b_2\lambda_1)\left(a_3a_4 - \lambda_{z2}^2\right)}{2a_2\lambda_2\lambda_{z1}a_4 - \left(a_1a_2 - \lambda_1^2\right)\left(a_3a_4 - \lambda_{z2}^2\right)}. \tag{29a}$$

Table 3: Mesh parameters of the ideal model for numerical simulation.

Grid parameters	Direction x	Direction y	Direction z
Number of grids	8	1	11
Grid step size (cm)	4	5	3

Table 4: Reservoir static parameters of the whole lithology ideal model.

Type	Subzone number	Lithology	k (10^{-3} μm^2)	Φ (%)	Net/gross	s_{wi}	p_i (atm)	$\bar{D}_p$ (MPa·m^{-1})	C_e ($\times 10^{-2}$ MPa^{-1})
Mudstone formations	1	Mudstone	0	2.98	1	0.7	30	—	—
	2				1			—	—
Transition layers	3	Sandy mudstone	0.5	11.47	1	0.7	30	0.307	0.14
	4				1			0.307	0.14
	5	Transition lithology	1	12.16	1	0.7	30	0.157	0.22
	6				1			0.157	0.22
	7				1			0.157	0.22
	8				1			0.157	0.22
Reservoir	9	Sandstone	3	14.68	1	0.35	30	0.024	0.38

The average reservoir pressure in the oil well controlled area is calculated as follows:

$$\bar{p}_{1o}^{n+1} = \frac{2a_2\lambda_1\lambda_2(b_3a_4 - b_4\lambda_{z2}) - \lambda_1(b_1a_2 + b_2\lambda_1)\left(a_3a_4 - \lambda_{z2}^2\right)}{2a_2^2\lambda_2\lambda_{z1}a_4 - \left(a_1a_2^2 - \lambda_1^2a_2\right)\left(a_3a_4 - \lambda_{z2}^2\right)}. \tag{29b}$$

The average pressure of transition lithology in the water well controlled area is calculated as follows:

$$\bar{p}_{2w}^{n+1} = \frac{(b_3a_4 - b_4\lambda_{z2})\left(a_1a_2 - \lambda_1^2\right)}{\lambda_{z1}a_4(b_1a_2 - b_2\lambda_1)}. \tag{29c}$$

The average pressure of mudstone formations in the water well controlled area is calculated as follows:

$$\bar{p}_{3w}^{n+1} = \frac{b_4}{a_4} + \frac{\lambda_{z2}(b_3a_4 - b_4\lambda_{z2})\left(a_1a_2 - \lambda_1^2\right)}{\lambda_{z1}a_4^2(b_1a_2 + b_2\lambda_1)}. \tag{29d}$$

The coefficients are $\bar{p}_{1w}^0 = \bar{p}_{1o}^0 = \bar{p}_{2w}^0 = \bar{p}_{3w}^0 = p_i$, when calculating $\bar{p}_{1w}^1$, $\bar{p}_{1o}^1$, $\bar{p}_{2w}^1$, and $\bar{p}_{3w}^1$. Therefore, the coefficients of the above formula have definite formulas. The average pressure everywhere can be calculated from time Δt_1, from which the remainder (Δt_2, Δt_3, Δt_4,…) can be deduced.

5. Model Validation and Application

5.1. Numerical Simulation Verification of the New Model. Although the commercial software Eclipse cannot simulate the water absorption characteristics of mudstone formations, the accurate pressure value predicted by Eclipse can be determined to be correct by setting an analytical water body to approximate the overflow and combining the historical fitting technology. Therefore, the numerical simulation results can be used as the evaluation criteria of the new model.

In this paper, the pressure prediction formula Equations (29a), (29b), (29c) and (29d) for an ultralow-permeability reservoir is validated by establishing an ideal model of the whole lithology numerical simulation. An ideal model containing 9 layers is established using the Eclipse numerical simulation software. The grid parameters are shown in Table 3, and the static reservoir parameters are shown in Table 4.

The ideal model is set to a constant flow production mode with a flow rate of 4.8 L/h, and the initial pressure of the reservoir is set at 30 atm. The comparison between the initial pressure profile of the ideal model and the pressure profile after stabilization is shown in Figure 7. The results of the Eclipse numerical simulation software and those of the new model are compared in Figure 8.

The verification results of the ideal model show that (1) under the condition of constant flow rate production, the pressure profile shows that the pressure of transition layers and mudstone at the end of the water well gradually increases, while the pressure at the end of the oil well basically remains unchanged, which is consistent with the hypothesis of the mathematical model established in this paper. (2) A higher injection-production ratio in the early stage of development is required to increase the pressure of the transition layers and mudstone formations at the water well end and gradually spread to the oil well end. (3) The pressure calculation results show that the new pressure prediction model established in this paper is consistent with the numerical simulation results.

5.2. Production Data Validation of the New Model. We take the actual production data of Chaoyang Gou Oilfield in

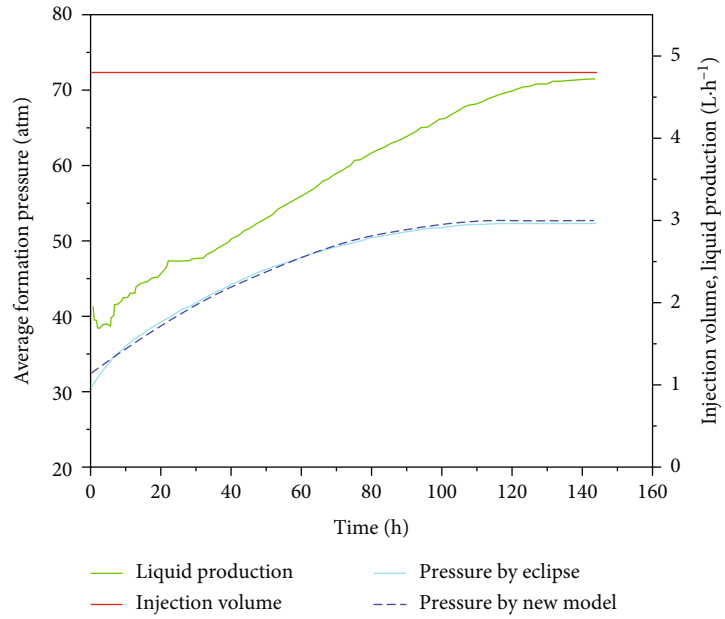

Figure 7: Relation of the injection-production and reservoir pressure calculated by different models.

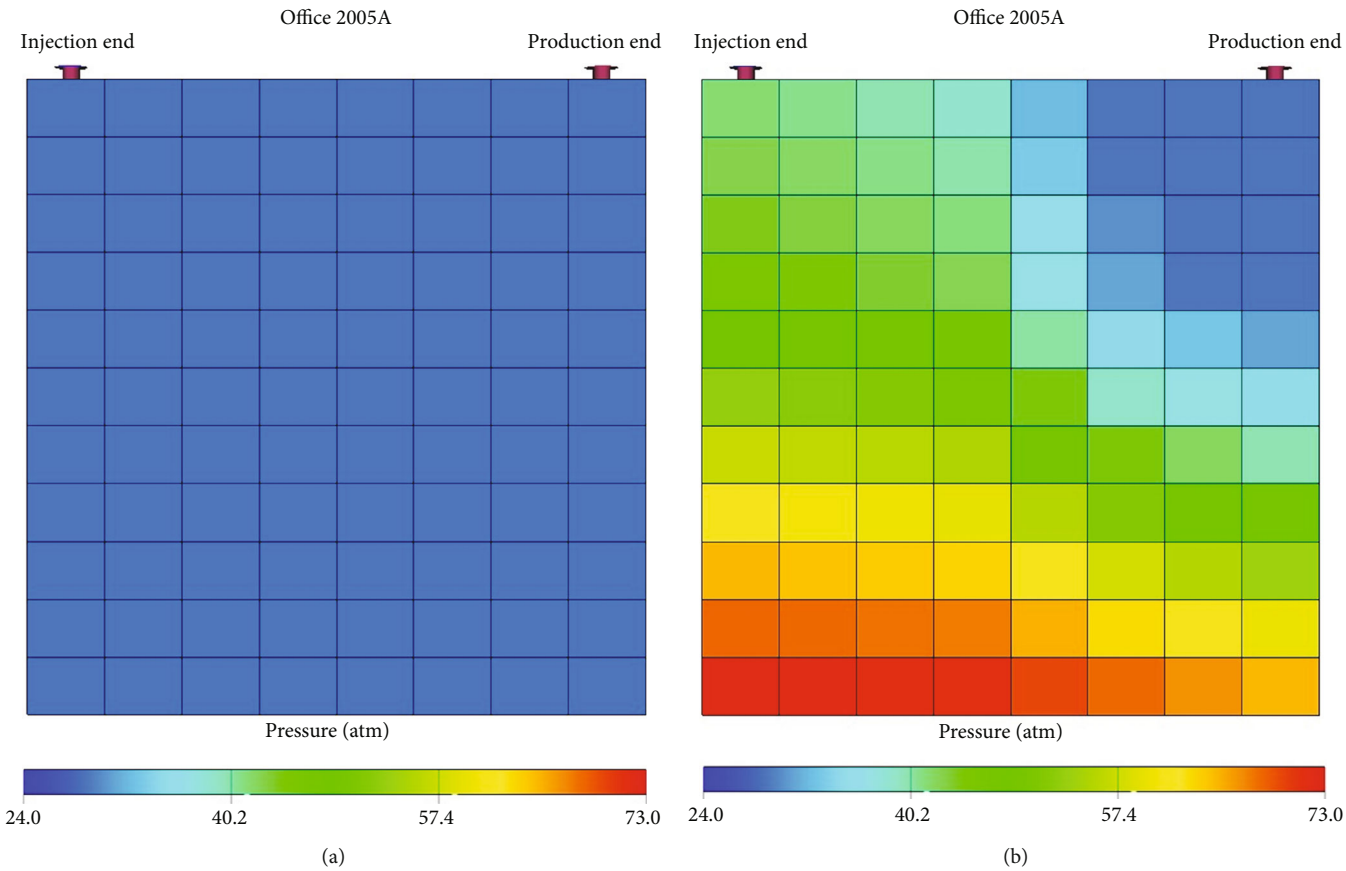

Figure 8: (a) Initial pressure profile; (b) pressure profile after stabilization.

China as the verification standard and use the average value of reservoir physical property parameters as the calculation basis of the theoretical model, as shown in Table 5. Under the conditions of different injection production ratios, the predicted average pressure in different areas of the whole lithologic reservoir is shown in Figure 9.

Table 5: Average value of the physical parameters of an actual reservoir.

	Mudstone formations	Sandy mudstones	Transition layers	Reservoir
Oil-water well spacing (m)	210	210	210	210
Thickness (m)	4.2	4.6	6.4	9.6
Threshold pressure gradient (MPa·m^{-1})	—	0.502	0.157	0.034
Porosity (%)	—	5.98	7.12	15.86
Permeability(10^{-3} μm^2)	—	0.124	0.542	4.453
Average elastic compression coefficient (10^{-2} MPa^{-1})	—	1.04	2.83	4.67

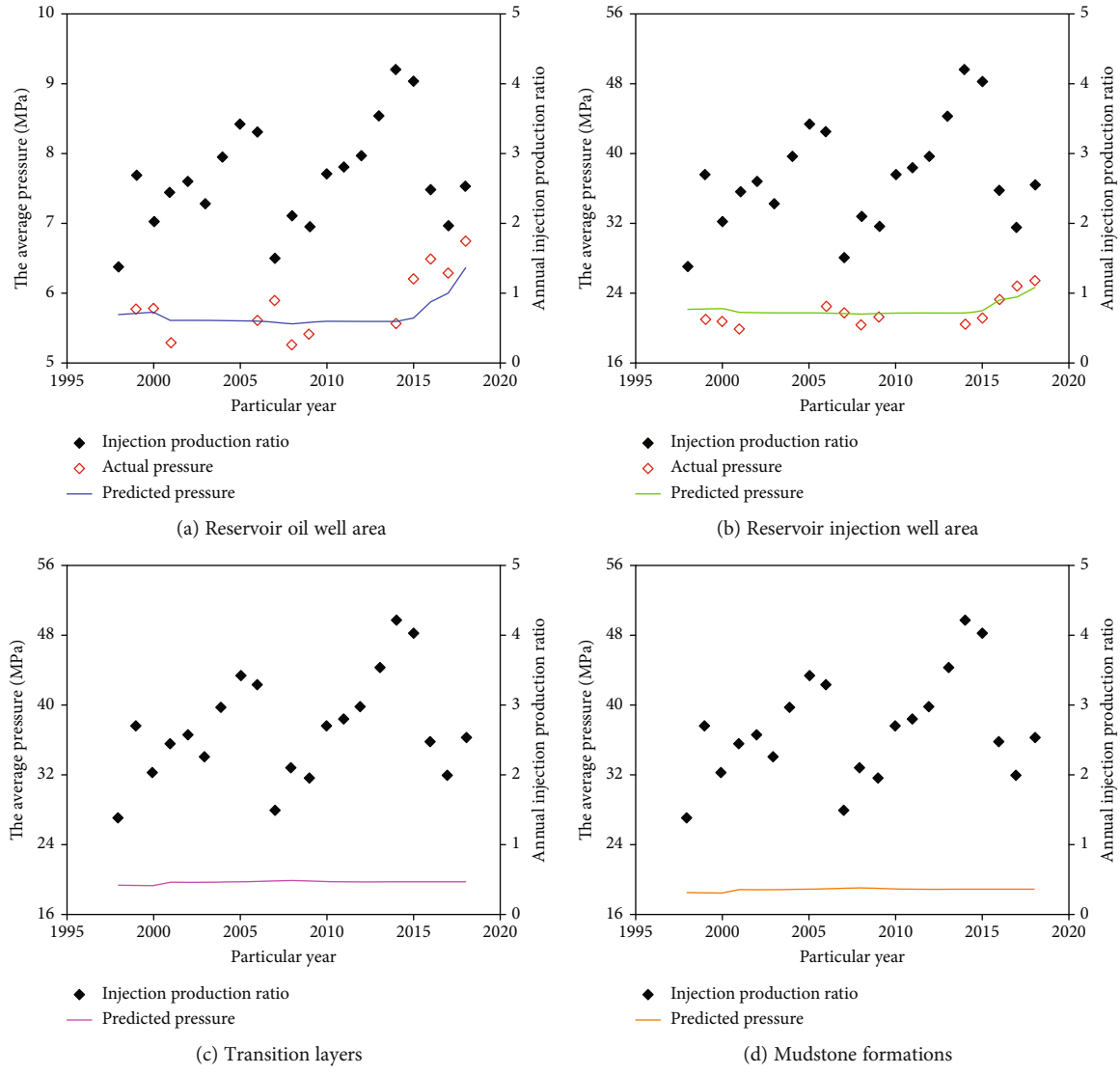

Figure 9: Production data validation results of the new pressure prediction model.

The results show that the average pressure of the oil well area and average pressure of the water well area calculated by the theoretical model are very consistent with the actual monitoring values; the average error is only 9.3%. The minimum oil well static pressure of the oil well area in the reservoir is 5.7 MPa, the maximum is 6.01 MPa, and the range of pressure change is small. However, the minimum injection well static pressure is 20.1 MPa, the maximum is 26.8 MPa, the overall range is maintained at 22.7 MPa, and the range of pressure change is large. The phenomena are mainly due to the extremely poor physical properties of the ultralow-permeability reservoir and poor connectivity between injection and oil wells. Even if the injection production ratio changes, the static pressure in the oil well area will not

significantly. Simultaneously, due to the serious pressure build-up in the water well area, the initial stage of water injection will maintain a high pressure, and a large amount of injected water under the effect of high pressure in the reservoir will successively enter the transition layers and mudstone formations.

6. Summary and Conclusions

(1) The water absorption characteristics of mudstone formations in ultralow-permeability reservoirs are defined through water absorption experiments of mudstone. The water absorption rate increases with the increase in water absorption time with the condition of constant water invasion pressure, but the increase gradually decreases. The saturation water absorption of mudstone increases with the increase in water invasion pressure, but the increase gradually decreases. The water absorption process of mudstone is quite different from the sandstone seepage process, so it cannot be described by the seepage equation

(2) An empirical function of negative exponential for the mudstone water absorption process is established based on the experimental results. The relation between saturation water absorption rate and water invasion pressure is logarithmic in the empirical function, and the relation between water absorption attenuation coefficient and water invasion pressure is a power function

(3) A new mathematical model of the whole lithologic is established. Combining the finite difference method and material balance method, the space terms in the basic differential equation are replaced by the material balance equation, and the finite difference of the time term is made. Then, the analytical solutions of the average pressure of different regions are solved by applying the research results of mudstone water absorption characteristics

(4) An ideal numerical simulation model is established, and the pressure profile shows that under the condition of constant flow rate production, the pressure of the transition layers and mudstone at the end of the water well gradually increases, while the pressure at the end of the oil well basically remains unchanged, which is consistent with the hypothesis of the mathematical model established in this paper. The verification results of oilfield production data show that the water well static pressure and oil well static pressure calculated by the new model are highly consistent with the actual value, which well explains the low reservoir pressure level at high injection production ratios in ultralow-permeability reservoirs

Nomenclature

R_{ws}: Water absorption rate varying with water invasion pressure and time (%)
R_{wsm}: Saturation water absorption (%)
δ: Water absorption attenuation coefficient (d^{-1})
t: Water absorption time (d)
P: Water invasion pressure (MPa)
P_i: Initial pressure (MPa)
Q: Cumulative water influx ($m^3 \cdot s^{-1}$)
q: Water invasion velocity per unit section area ($m \cdot s^{-1}$)
S: Section area (m^2)
d: Water invasion distance perpendicular to cross section (m)
φ_1: Porosity of reservoir
p_1, p_2, p_3: Fluid pressure of reservoir, transition lithology, and sandy mudstone (MPa)
D_p: Threshold pressure gradient ($MPa \cdot m^{-1}$)
$\bar{p}_{1w}$, $\bar{p}_{1o}$: Average formation pressure of reservoir in the area controlled by water and oil wells (MPa)
$\bar{p}_{2w}$, $\bar{p}_{3w}$: Average pressure of transition layers and mudstone formations in the well control area (MPa)
V_{w1}, V_{o1}: Volume of reservoir within the control range of water and oil wells (m^3)
V_{w2}, V_{w3}: Volume of transitional lithology and sandy mudstone in the controlled range of the water well (m^3)
q_w, q_L: Injection rate of the water well and fluid production of the oil well ($m^3 \cdot d^{-1}$)
q_{wi}, q_{lj}: Water injection intensity of water well and fluid production intensity of oil well ($(m^3 \cdot (d \cdot m)^{-1}$)
q_{k1}, q_{k2}, q_{k3}: Water absorption intensity of transitional lithology, sandy mudstone, and mudstone ($(m^3 \cdot (d \cdot m^2)^{-1}$)
q_{k4}: Transfer intensity of unclosed spillover of sandy mudstone ($(m^3 \cdot (d \cdot m^2)^{-1}$)
λ_1, λ_{z1}, λ_{z2}, λ_{z3}: Conductivity in reservoir, conductivity from reservoir to transition lithology, conductivity from transition lithology to sandy mudstone, and conductivity from sandy mudstone to mudstone
$\bar{k}_1$, $\bar{k}_2$: Average permeability from the middle of the reservoir to the middle of the transition lithology and average permeability from the middle transition lithology to the middle of the sandy mudstone ($10^{-3}\,\mu m^2$)
$\bar{D}_{p1}$, $\bar{D}_{p2}$: Average threshold pressure gradient from the middle reservoir to the middle of the transition lithology and average threshold pressure gradient from the middle of the transition lithology to the middle of the sandy mudstone (MPa/m)
C_{e1}, C_{e2}, C_{e3}: Total compressibility of the reservoir, transition lithology and sandy mudstone (MPa^{-1})
A: Cross-section area of flow (m^2)
L: Distance between the center of the water well controlled area and the center of the oil well controlled area (m)
s_1, s_2, s_3: Cross-section area of transition lithology, sandy mudstone, and mudstone (m^2)

h_1, h_2, h_3: Thickness of the reservoir, transition lithology, and sandy mudstone (m)

d_1, d_2, d_3: Distance from the middle of the reservoir to the middle of the transition lithology, from the middle of the transition lithology to the middle of the sandy mudstone, and from the top of the sandy mudstone to the middle of the mudstone (m)

Data Availability

The data used to support the findings of this study are available from the corresponding author upon request.

Conflicts of Interest

The authors declare that they have no conflicts of interest.

Acknowledgments

This work was funded by the Ministry of Science and Technology of the People's Republic of China, and the name of the project is "Demonstration Project for Development of Dense Oil in Jiyang Depression, Bohai Bay Basin (2017ZX05072)" of the National Science and Technology Major Special Project.

References

[1] T. A. Blasingame, "The characteristic flow behavior of low-permeability reservoir systems," in *SPE Unconventional Reservoirs Conference*, Keystone, Colorado, USA, February 2008.

[2] A. Kumar, R. G. Dusterhoft, and S. Siddiqui, "Completion and production strategies for liquids-rich wells in ultra-low-permeability reservoirs," in *SPE Annual Technical Conference and Exhibition*, New Orleans, LA, USA, September-October 2013.

[3] F. Ma, S. He, H. Zhu, Q. Xie, and C. Jiao, "The effect of stress and pore pressure on formation permeability of ultra-low-permeability reservoir," *Petroleum Science and Technology*, vol. 30, no. 12, pp. 1221–1231, 2012.

[4] W. Y. Zhu, Y. Ju, M. Zhao, Q. Chen, and Z. H. M. Yang, "Spontaneous imbibition mechanism of flow through porous media and waterflooding in low-permeability," *Acta Petrolei Sinica*, vol. 6, pp. 56–59, 2002.

[5] J. Liu, X. Yu, and J. Zhao, "Numerical simulation of geostress and pore pressure evolution around oil or water well under different injection-production ratio," *Mathematical Problems in Engineering*, vol. 2013, Article ID 604748, 10 pages, 2013.

[6] X. P. Fan, X. R. Xu, and S. C. Zhang, "Analysis on changes of stress, strain, porosity and permeability in multiphase reservoir with fluid-solid coupled and geomechanical mathematic simulation," *Rock and Soil Mechanics*, vol. 22, pp. 47–50, 2001.

[7] R. L. Johnson and J. L. Rodgerson, "More effective hydraulic fracturing in secondary, in-fill developments, Permian Basin, using bottomhole pressure and in-situ stress profiling techniques," in *SPE Permian Basin Oil and Gas Recovery Conference*, pp. 281–296, Midland, TX, USA, March 1998.

[8] Z. M. Yin, Q. Wu, J. J. Liu, and C. H. Yang, "Numerical simulation of geostress distribution during injecting well blowout," *Rock and Soil Mechanics*, vol. 25, pp. 363–368, 2004.

[9] C. Zou, Y. Chang, G. Wang, and L. Lan, "Calculation on a reasonable production/injection well ratio in waterflooding oilfields," *Petroleum Exploration and Development*, vol. 38, no. 2, pp. 211–215, 2011.

[10] Q. Wu, "Study on the mechanism of high injection-production ratio (IPR) for low-permeability oil reservoirs," *Special Oil & Gas Reservoirs*, vol. 19, pp. 82–85, 2012.

[11] P. Liu, Z. Na, H. Manchao, L. Dejian, and T. Qimin, "Experimental study on water absorption processes of sandy mudstone in Pingzhuang coal mine," *Metal Mine*, vol. 9, pp. 49–53, 2011.

[12] B. Vásárhelyi and P. Ván, "Influence of water content on the strength of rock," *Engineering Geology*, vol. 84, no. 1-2, pp. 70–74, 2006.

[13] L. N. Y. Wong, V. Maruvanchery, and G. Liu, "Water effects on rock strength and stiffness degradation," *Acta Geotechnica*, vol. 11, no. 4, pp. 713–737, 2016.

[14] L. Wang, W. Zhang, and F. Chen, "Bayesian approach for predicting soil-water characteristic curve from particle-size distribution data," *Energies*, vol. 12, no. 15, article 2992, 2019.

[15] Y. Lu, L. Wang, X. Sun, and J. Wang, "Experimental study of the influence of water and temperature on the mechanical behavior of mudstone and sandstone," *Bulletin of Engineering Geology and the Environment*, vol. 76, no. 2, pp. 645–660, 2017.

[16] Q. Jiang, B. Yang, F. Yan, C. Liu, Y. Shi, and L. Li, "New method for characterizing the shear damage of natural rock joint based on 3D engraving and 3D scanning," *International Journal of Geomechanics*, vol. 20, no. 2, article 06019022, 2020.

[17] Q. Jiang, G. Su, X. T. Feng, G. Chen, M. Z. Zhang, and C. Liu, "Excavation optimization and stability analysis for large underground caverns under high geostress: a case study of the Chinese Laxiwa project," *Rock Mechanics and Rock Engineering*, vol. 52, no. 3, pp. 895–915, 2019.

[18] Z. A. Erguler and R. Ulusay, "Water-induced variations in mechanical properties of clay-bearing rocks," *International Journal of Rock Mechanics and Mining Sciences*, vol. 46, pp. 355–370, 2009.

[19] Q. Jiang, J. Cui, X. T. Feng, and Y. Jiang, "Application of computerized tomographic scanning to the study of water-induced weakening of mudstone," *Bulletin of Engineering Geology and the Environment*, vol. 73, no. 4, pp. 1293–1301, 2014.

[20] L. Dejian, W. Guilian, H. Liqiang et al., "Analysis of microscopic pore structures of rocks before and after water absorption," *Mining Science and Technology*, vol. 21, no. 2, pp. 287–293, 2011.

[21] H. Guo, X. Lei, Y. Zhang, G. Yang, and Z. Niu, "Experimental research on hydrophilic characteristics of natural soft rock at high stress state," *International Journal of Mining Science and Technology*, vol. 25, no. 3, pp. 489–495, 2015.

[22] M. C. He, L. Zhou, D. J. Li, C. G. Wang, and W. Nie, "Experimental research on hydrophilic characteristics of mudstone in deep well," *Chinese Journal of Rock Mechanics and Engineering*, vol. 27, pp. 1113–1120, 2008.

[23] N. Hao, Y. L. Wang, Q. X. ZH, X. L. Zhang, W. F. Liu, and H. MCH, "Experimental study on water absorption characteristic and salt enrichment of mudstone at Mogao Grott," *Coal Technology*, vol. 37, pp. 308–310, 2018.

[24] T. B. Boving and P. Grathwohl, "Tracer diffusion coefficients in sedimentary rocks: correlation to porosity and hydraulic conductivity," *Journal of Contaminant Hydrology*, vol. 53, no. 1-2, pp. 85–100, 2001.